

Surface enhanced Raman scattering of pyridine adsorbed on Au@Pd core/shell nanoparticles

Zhilin Yang,^{1,2} Yan Li,² Zhipeng Li,¹ Deyin Wu,³ Junyong Kang,^{2,4} Hongxing Xu,^{1,5} and Mengtao Sun^{1,a)}

¹Beijing National Laboratory for Condensed Matter Physics, Institute of Physics, Chinese Academy of Sciences, P.O. Box 603-146, Beijing 100190, People's Republic of China

²Department of Physics, Xiamen University, Xiamen 361005, People's Republic of China

³State Key Laboratory of Physical Chemistry of Solid Surfaces and Department of Chemistry, College of Chemistry and Chemical Engineering, Xiamen University, Xiamen 361005, People's Republic of China

⁴Fujian Key Laboratory of Semiconductors and Applications, Xiamen University, Xiamen 361005, People's Republic of China

⁵Division of Solid State Physics, Lund University, Lund 22100, Sweden

(Received 18 March 2009; accepted 21 May 2009; published online 18 June 2009)

Surface enhanced Raman scattering (SERS) of pyridine adsorbed on Au@Pd core/shell nanoparticles has been investigated theoretically with quantum chemical method, generalized Mie theory and three-dimensional finite-difference time domain (3D-FDTD) method. We first studied the influence of the coated Pd on the electronic structure of Au nanoparticle, and compared the electronic structure of Au₂₀ cluster with that of Au₁₀Pd₁₀ (core/shell) cluster. Second, we studied SERS spectroscopy of pyridine on Au@Pd core/shell nanoparticles, which revealed the rate of static chemical enhancement and electromagnetic enhancement in the experimental reports. Third, the influence of the Pd shell thickness to the optical absorption of Au@Pd core/shell nanoparticles was investigated with generalized Mie theory. Fourth, we studied the influence of the shell thickness to the local electric field enhancement with 3D-FDTD method. The theoretical results reveal that the static chemical enhancement and electromagnetic enhancement are in the order of 10 and 10³, respectively. These theoretical studies promote the deeper understanding of the electronic structure and optical absorption properties of Au@Pd, and the mechanisms for SERS of molecule adsorbed on Au@Pd. © 2009 American Institute of Physics. [DOI: 10.1063/1.3153917]

I. INTRODUCTION

Since the discovery of surface enhancement Raman scattering (SERS),¹⁻³ it has been extensively studied experimentally and theoretically⁴⁻¹⁰ because of its extremely high surface sensitivity and powerful application on fingerprint vibrational spectroscopy in qualitative and quantitative analysis. Before the mid-1990s, most investigation focused on the three “coinage metals” (Au, Ag, and Cu), since they can provide the large enhancement via surface plasmon resonance (SPR). Since the mid-1990s, SERS for different transition metals has been investigated gradually, because of the importance of transition metal (VIII B group elements) in electrochemistry and catalyst.¹⁰⁻¹³ The SERS signals on the transition metals are rather weak or even below the detection limit from some adsorbates with a very small Raman cross section or with a low surface coverage because of the lack of SPR features in the visible spectral region. The best way is to further increase the SERS activity of transition metal utilizing the long-range effects of electromagnetic enhancements created by SERS-active Au or Ag substrates underneath an ultrathin layer of transition metals.^{10,14-19} Experimentally, the many core/shell nanoparticles, such as Au@Pd and Au@Pt,

have been successfully synthesized, and strong SERS signals have been obtained.^{10,14-19} Theoretically, structure and optical properties of the nanoalloys Ag₃Au₁₀ have been theoretically studied by a combination of genetic algorithm global optimization and density functional theory calculations.²⁰

The pyridine molecule is an important probe molecule in SERS field. The enhancement effect is strongly dependent on the SERS substrates. On the basis of density functional theory (DFT) calculations, the enhancement effect has been studied for pyridine interacting with small silver, gold, and copper clusters. The results indicated that the adsorption interaction not only results in the significant shift in vibration frequencies, but also changes its relative Raman intensities. The studies provided for us to understand the binding interaction and adsorption orientation of surface species. Recently, SERS of pyridine adsorbed on much larger clusters Au₂₀ nanoparticles,²¹ Ag₂₀ nanoparticles,⁸ or in Ag hydrosols²² have been also studied theoretically, while investigations on the SERS of the molecule adsorbed on the core/shell nanoparticles is few and is imminently needed. On gold core/transition metal shell nanoparticles, the enhancement factor can be promoted to two orders of magnitude with respect to the pure transition metal nanoparticles in a sphere shape with the same size. However, the nature of the enhancement effect was thought due to the long-range effect from the electromagnetic enhancement. In fact, the chemical

^{a)}Author to whom correspondence should be addressed. Electronic mail: mtsun@aphy.iphy.ac.cn.

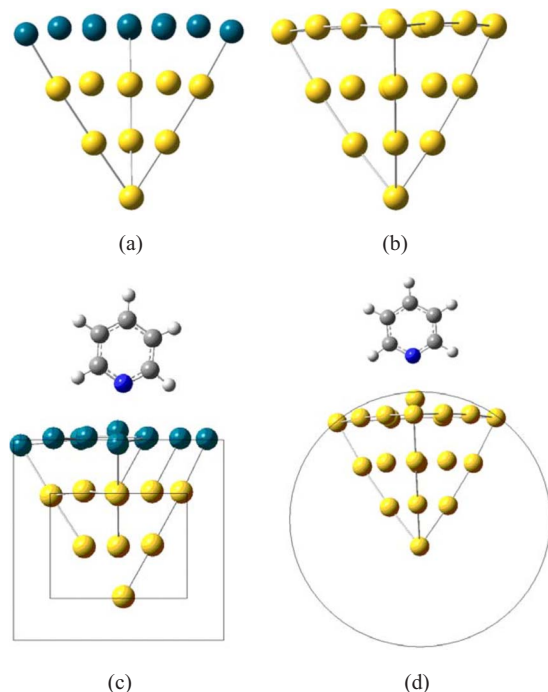


FIG. 1. (Color online) Chemical structure of (a) $\text{Au}_{10}\text{Pd}_{10}$, (b) Au_{20} , (c) pyridine- $\text{Au}_{10}\text{Pd}_{10}$, and (d) pyridine- Au_{20} .

enhancement effect cannot be neglected. The shell of the coated transition metal in electronic structures is very sensitive to the core metal. Therefore, the surface binding interaction of pyridine interacting with the transition metals plays an important role in understanding the SERS mechanism of pyridine adsorbed on the core/shell nanoparticles.

We have theoretically investigated the enhancement mechanism on SERS of pyridine adsorbed on the Ag nanoparticles^{23,24} with quantum chemical theory, generalized Mie theory,²⁵ and three-dimensional finite-difference time domain (3D-FDTD) method,^{13,26} where the effects of quantum size and binding site on SERS have been clearly shown, and regions of electromagnetic and chemical enhancements in the excitation wavelengths ranging from 300 to 1000 nm have been successfully clarified with charge difference density. We also investigated the chemical enhancement mechanism [charge transfer (CT) mechanism] on the SERS in metal-PATP (para-aminothiophenol)-metal junction with quantum chemical method, in which the tunneling CT at the incident light of 1064 nm has been visualized with charge difference density.²⁷

In this paper, we extend our theoretical investigation on the SERS of molecule adsorbed on the core/shell nanoparticles with quantum chemical method, generalized Mie theory and 3D-FDTD method, where pyridine (Py) and Au@Pd were chosen as the molecule and core/shell nanoparticles, respectively.

II. METHODS

The models of $\text{Au}_{10}\text{Pd}_{10}$ tetrahedral as a part of Au@Pd, and Au_{20} tetrahedral as a part of a pure gold nanoparticle (a part of nanosphere or nanocube) have been chosen, which can be seen from Fig. 1. Recent photoelectron spectroscopy

and relativistic density functional calculations strongly predict that Au_{20} has a tetrahedral geometry similar to a fragment of bulk face-centered cubic gold.²⁸ Several theoretical studies have revealed that the absorption properties of a 20 atom silver or gold tetrahedral cluster behave quite similar to the plasmon excitation observed in nanoparticles, and the Raman enhancement due to this cluster is comparable to that from large nanoparticles (>10 nm).^{8,21,29} The Au@Pd nanocubes with different Pd shell have been synthesized experimentally.³⁰

All the quantum chemical calculations were done with GAUSSIAN03 suite.³¹ The ground state geometries of $\text{Au}_{10}\text{Pd}_{10}$ tetrahedral, Au_{20} tetrahedral, pyridine- $\text{Au}_{10}\text{Pd}_{10}$ complex, and pyridine- Au_{20} complexes were optimized with DFT,³² B3LYP functional,³³ and LanL2DZ basis set.³⁴ It should be noted that $\text{Au}_{10}\text{Pd}_{10}$ tetrahedral, Au_{20} tetrahedral, and pyridine- Au_{20} complexes were fully optimized, while the optimized $\text{Au}_{10}\text{Pd}_9$ tetrahedral was frozen for the optimization of pyridine- $\text{Au}_{10}\text{Pd}_{10}$ complex (the Pd at the surface center and pyridine as well as the frozen $\text{Au}_{10}\text{Pd}_9$ were optimized). The partial density of state (PDOS) and energy levels of occupied and unoccupied molecular orbitals of them were analyzed with GAUSSSUM software.³⁵ The static normal Raman scattering (NRS) spectra of pyridine- $\text{Au}_{10}\text{Pd}_{10}$ complex was calculated at the same theoretical level. Optical absorption spectrum was calculated with time-dependent DFT method.³⁶ Distribution of electron-hole pairs in pyridine- $\text{Au}_{10}\text{Pd}_{10}$ on electronic excitations were visualized with charge difference density. The influence of the Pd shell thickness to the extinction spectrums of Au@Pd core/shell nanoparticles was investigated with generalized Mie theory.^{37,38}

The 3D-FDTD method was used for the theoretical simulation of the local electric field on Au@Pd nanocube dimers. FDTD method is a powerful computational technique which is widely used to simulate the optical properties of plasmonic nanostructures with arbitrary size and shape.²⁶ An important requirement of this method for the study of dispersive material, such as gold or palladium, is the need of an analytical law of dispersion. It is known that the Drude model can not accurately describe the frequency-dependent complex permittivity for metals over a wide frequency range, especially for gold since the interband transitions play an

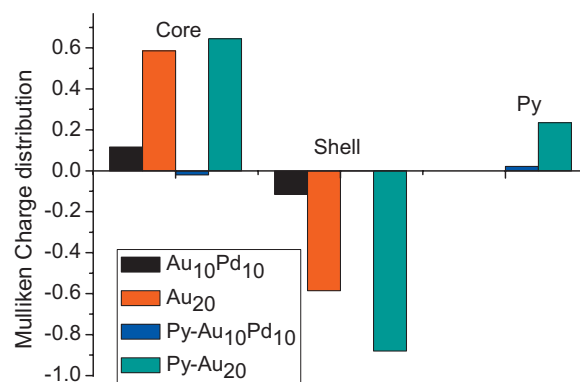


FIG. 2. (Color) Mulliken charge distributions at ground state for $\text{Au}_{10}\text{Pd}_{10}$, Au_{20} , pyridine- $\text{Au}_{10}\text{Pd}_{10}$, and pyridine- Au_{20} .

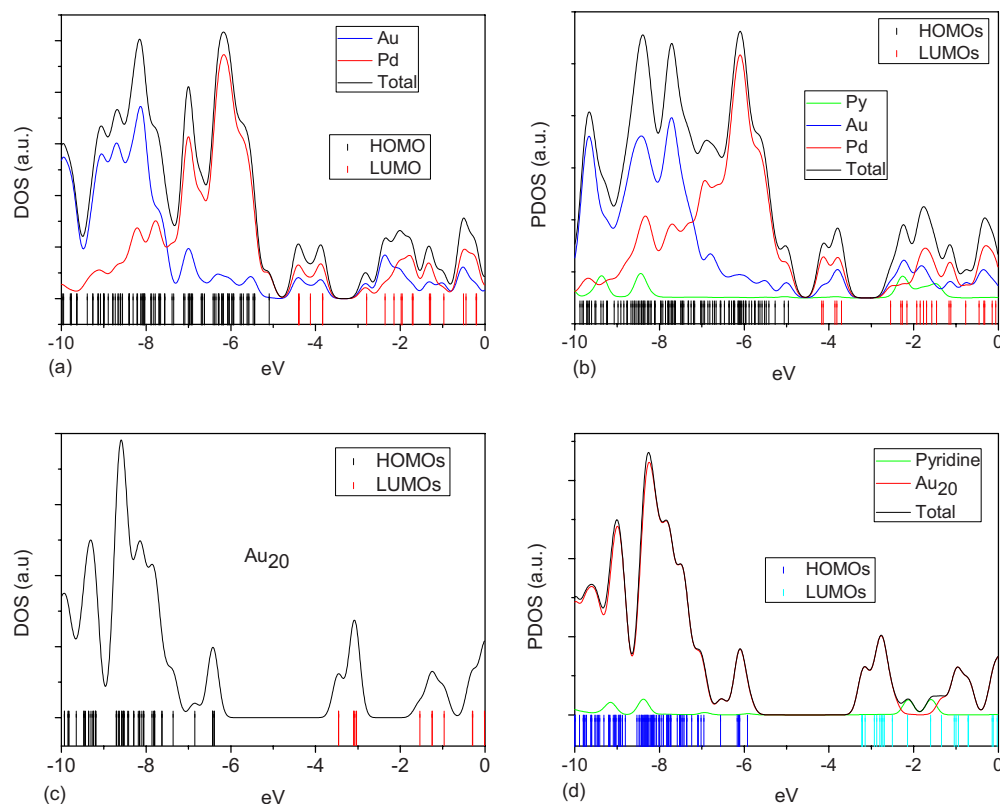


FIG. 3. (Color online) Partial density of state (PDOS) for (a) $\text{Au}_{10}\text{Pd}_{10}$, (b) Au_{20} , (c) pyridine- $\text{Au}_{10}\text{Pd}_{10}$, and (d) pyridine- Au_{20} .

important role in the dielectric function. In recent years, some efficient analytical models have been developed to describe the dielectric response of dispersive materials.^{39–42} In this work, instead of the simple Drude model, we adopted the general Drude model to simulate the complex permittivity of gold and palladium with the form of^{42,43}

$$\varepsilon(\omega) = \varepsilon_{\infty} + \frac{\varepsilon_s - \varepsilon_{\infty}}{1 + i\omega\tau} + \frac{\sigma}{i\omega\varepsilon_0}, \quad (1)$$

where ε_s , ε_{∞} , σ , and τ represent static permittivity, infinite frequency permittivity, conductivity, and the relaxation time, respectively, ω is the angular frequency, and ε_0 is the permittivity of free space. The four parameters ε_s , ε_{∞} , σ , and τ can be adjusted through curve-fitting techniques to correctly match the complex permittivity which can be derived from the experimentally determined optical constants through the relationship $\varepsilon_r = n^2 - k^2$ and $\varepsilon_i = 2nk$, where ε_r and ε_i are the real and imaginary parts of dielectric function of the dispersive material, respectively. This model for the local dielectric function of metallic materials represents faithfully the optical response in a wide frequency region, especially at visible frequencies, ensuring the accuracy of the FDTD simulation.^{42,43} The experimental optical constant data are taken from Refs. 44 and 45.

To accurately simulate the detailed nanostructure of Au@Pd nanocubes, nonuniform FDTD mesh method was adopted in our calculations. This method could save computation resources greatly without losing the accuracy. The number of periods of the incident sinusoidal plane wave was set to 12 to guarantee calculation convergence, which could be judged by checking whether near zone electric field val-

ues had reached a steady state. The amplitude of the sinusoidal plane wave was set to be 1 V/m in the calculation, and the excitation wavelength is 632.8 nm. All FDTD calculations were conducted in the platform of a commercial XFDTD software package (RemCom XFDTD 6.3)

III. RESULTS AND DISCUSSION

The Mullikan charge distributions on Au_{20} , $\text{Au}_{10}\text{Pd}_{10}$, Py-Au_{20} , and $\text{Py-Au}_{10}\text{Pd}_{10}$ at the ground state can be seen from Fig. 2. For Au_{20} and $\text{Au}_{10}\text{Pd}_{10}$ tetrahedrals, electrons and holes are distributed on the shell and core, respectively. The amount of electrons on Au surface is 5.1 times than electrons on the surface of the Pd shell, so the electromagnetic (EM) enhancement of core-shell structure should be less than that of Au nanoparticle when they are of the same size and shape. Because of the interactions between pyridine and nanoparticles, the charges will be redistributed. For Py-Au_{20} , 0.24 electrons on Py and 0.06 electrons on Au core are simultaneously transferred to the surface of cluster. For $\text{Py-Au}_{10}\text{Pd}_{10}$, the electrons on Py and on Pd shells are simultaneously transferred to the core, and there is almost no net electron at the Pd shell. So, the EM enhancement for Au@Pd should mostly be contributed from the Au core. By comparing the charges on Py for Py-Au_{20} (see Fig. 2), $\text{Py-Au}_{10}\text{Pd}_{10}$, we can see that the Pd shell hampered the charges transfer, the rate of transferred electrons from Py to $\text{Au}_{10}\text{Pd}_{10}$ is only 9% than the rate in Py-Au_{20} .

We also studied the DOS for Au_{20} , $\text{Au}_{10}\text{Pd}_{10}$, Py-Au_{20} , and $\text{Py-Au}_{10}\text{Pd}_{10}$ (see Fig. 3). By comparing the PDOS of $\text{Au}_{10}\text{Pd}_{10}$ with that of Au_{20} , two conclusions can be drawn.

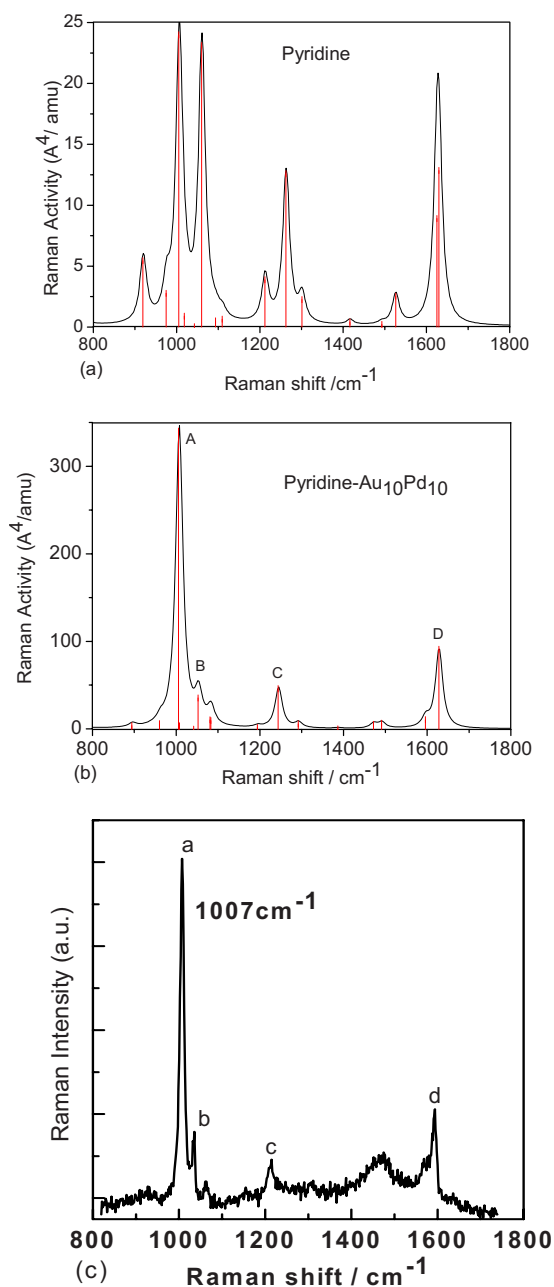


FIG. 4. (Color online) (a) Calculated NRS spectroscopy of isolated pyridine, (b) calculated NRS spectroscopy of pyridine adsorbed on Au@Pd, and (c) SER spectra of pyridine adsorption on 120 nm Au at 0.35 nm Pd/GC at -0.6 V in 0.1 M NaClO₄ and 1 mM pyridine, which is from Ref. 47.

The band gap ($\Delta E_{\text{bg}} = E_{\text{HOMO}} - E_{\text{LUMO}}$) (HOMO denotes highest occupied molecular orbital and LUMO denotes lowest unoccupied molecular orbital) of Pd₁₀Au₁₀ (0.70 eV) is significantly smaller than that of Au₂₀ (2.93 eV), due to the strong activity of the Pd shell. So, the edge of optical absorption of Pd₁₀Au₁₀ should be significantly redshifted, compared to that of Au₂₀. PDOS of Au₁₀Pd₁₀ between -6.4 eV (the energy level of HOMO of Au₂₀) and -3.47 eV (the energy level of LUMO of Au₂₀) are mostly contributed from Pd. By checking the DOS, the lowest resonant electronic transition for CT excitation (density are localized on cluster for HOMO, and lowest LUMOs that density are localized on Py) is 2.66 eV and 2.90 eV for Py-Pd₁₀Au₁₀ and Py-Au₂₀, respectively. Then, the thin Pd shell only slightly red shifted about

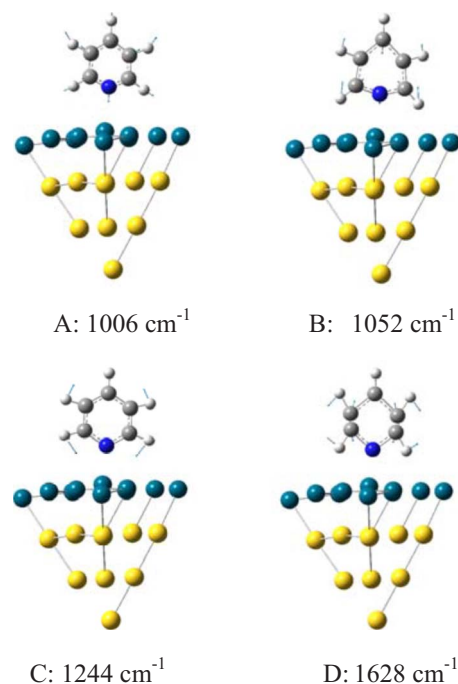


FIG. 5. (Color online) Normal modes of selected frequencies for pyridine adsorbed on Au@Pd.

0.24 eV of the CT transition energy. In the energy region from 0.73 eV (the band gap of Py-Pd₁₀Au₁₀) to 2.66 eV, they should be the intracluster resonant electronic transitions for Py-Pd₁₀Au₁₀. In the energy region from 2.70 eV (the band gap of Py-Au₂₀) to 2.90 eV, all transitions should be the intracluster resonant excitations of Py-Au₂₀.

We calculated the static NRS spectroscopy and compared it with the experimental results (see Fig. 4). We see that the calculated results are well consistent with the experimental report. There are four important peaks, which are 1006 (ring breathing with N moving toward cluster), 1052 (trigonal ring deformation), 1244 (C-H in-plane bending), and 1628 cm⁻¹ (mainly of C-C stretching with the α -carbon next to nitrogen vibrating toward the cluster), which can be seen from Fig. 5. Comparison the NRS intensities of Py-Au₁₀Pd₁₀ with those of isolated Py indicates that the static chemical enhancement via the CT results in the intensity enhancement factor of 12.1, 1.6, 3.7, and 7.1, respectively. The difference of the enhancements between the normal mode of 1006 cm⁻¹ and the normal mode of 1052 cm⁻¹ also results from the bonding interaction between metal and N atom of Py,⁴⁶ since the movement of N is toward the cluster for the normal mode of 1006 cm⁻¹. Experimentally, the enhancement factor for the 135 nm Au at 0.7 nm Pd was estimated to be about 5×10^4 at the incident light of 632.8 nm.⁴² Accordingly, we can estimate that the static chemical enhancement is about 10, and SERS enhancement contributed from EM at the incident light of 632.8 nm should be about 5×10^3 . In the SERS experiment at the incident light of 632.8 nm, there is no resonant CT (between Py and Au@Pd cluster) enhancement, because the lowest excitation energy for a CT excitation is 2.66 eV (466 nm), which is from an intracluster resonant electronic transition.

To study the optical excitation properties around 633 nm,

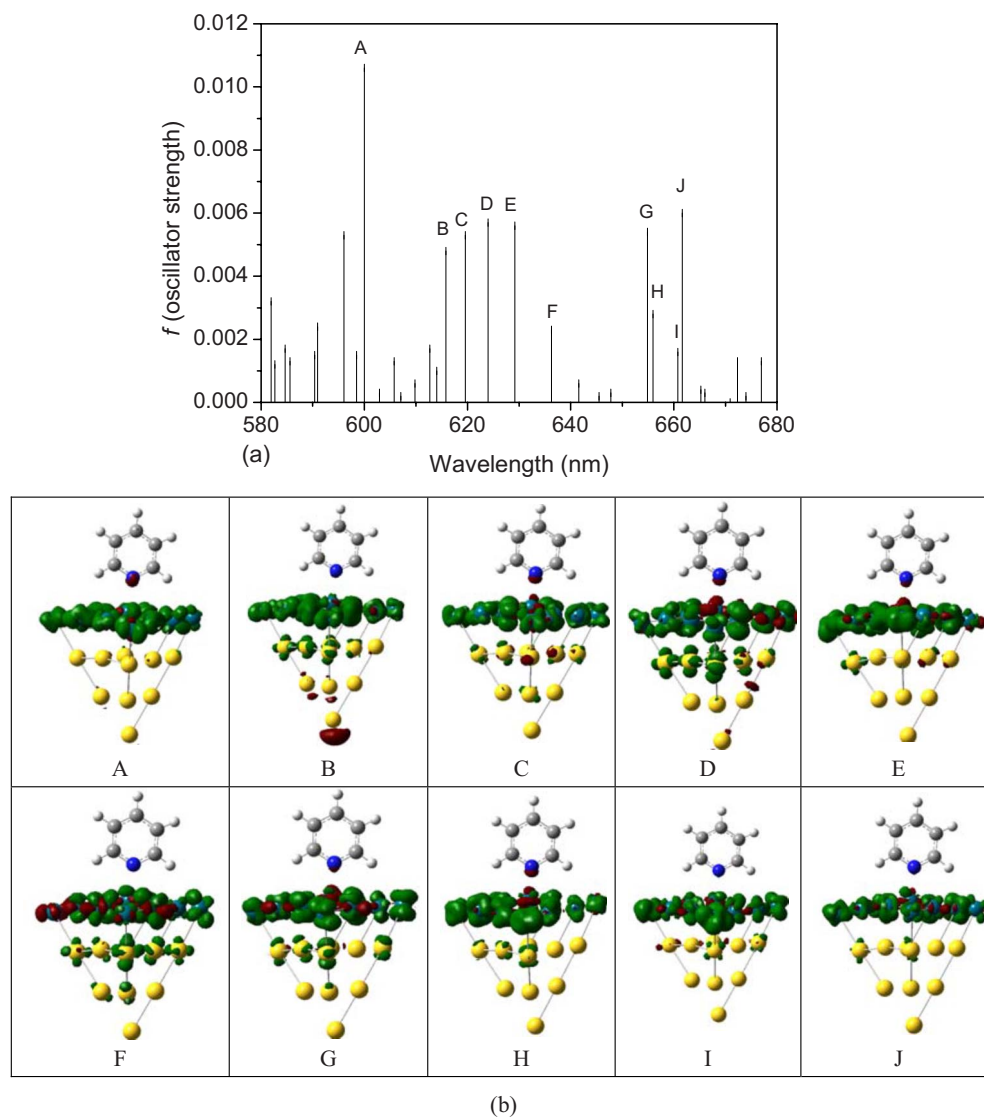


FIG. 6. (Color online) (a) Optical absorption spectrum around 633 nm (633 ± 50 nm) and (b) charge difference densities for ten excited states (A–J), where the green and red stand for hole and electron, respectively.

the distributions of electron-hole pairs between 600 and 660 nm were visualized with charge difference density. The optical absorption can be seen from Fig. 6(a), photoinduced charge redistribution on ten important excited states with the high oscillator strength reveal that they are the first Pd layer excitation, where the electrons and holes are all located in the first Pd layer [see Fig. 6(b)]. The electron-hole pairs in the first Pd layer are a kind of surface plasmon coming from transition metal. The mentioned results show that the SERS spectrum of pyridine adsorbed on the Au@Pd at the incident light of 632.8 nm should be contributed from the static chemical enhancement by the CT from pyridine to Au core at the ground state, the long-range effect of the enhanced electromagnetic field generated by the Au core, and the photoinduced charge redistribution at first Pd layer.

Due to the limitation of high computational demand, it is difficult to study the influence of the shell thickness to the optical absorption and EM enhancement of SERS with electronic structure methods. To study the influence of the shell

thickness to the optical absorption and EM enhancement of SERS, the generalized Mie theory and 3D-FDTD methods were employed, respectively.

The influence of the Pd shell thickness on the extinction spectra of Au@Pd Core/Shell Nanoparticles was investigated with generalized Mie theory. A series of extinction spectra of Au@Pd nanoparticles with a fixed core size of 120 nm and varying shell thicknesses were calculated using generalized Mie theory (see Fig. 7). The spectrum of the corresponding Au core is also given for reference. It can be seen that as the Pd shell becomes thicker, the absorption peak of the Au core slightly red-shifts and damps gradually. The calculated results were consistent with the experimental report in Ref. 47.

Au@Pd nanocubes with well-controllable ultrathin shell has been shown as excellent SERS substrate.³⁰ Experimental results show that the SERS intensity decays exponentially with the increase in Pd shell thickness, and reaches a constant value at ca. 2 nm. To quantitatively account for the SERS activity of the Au@Pd core-shell nanocubes system, we use the 3D-FDTD method to calculate electromagnetic

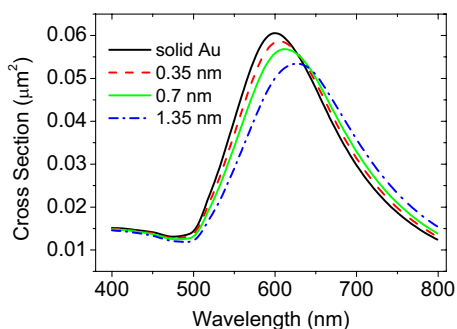


FIG. 7. (Color online) The calculated extinction spectra of 120 nm Au nanoparticle (black), Au@Pd particle with the thickness of Pd shell 0.35 nm (red dashed line), 0.7 nm (green solid line), and 1.35 nm (blue dot-dashed line), respectively.

field distribution around the illuminated nanocubes. It is well known EM model in terms of single particle is a poor model for SERS-active nanoparticle aggregates system, any simulations for the EM enhancement for a real SERS-active sys-

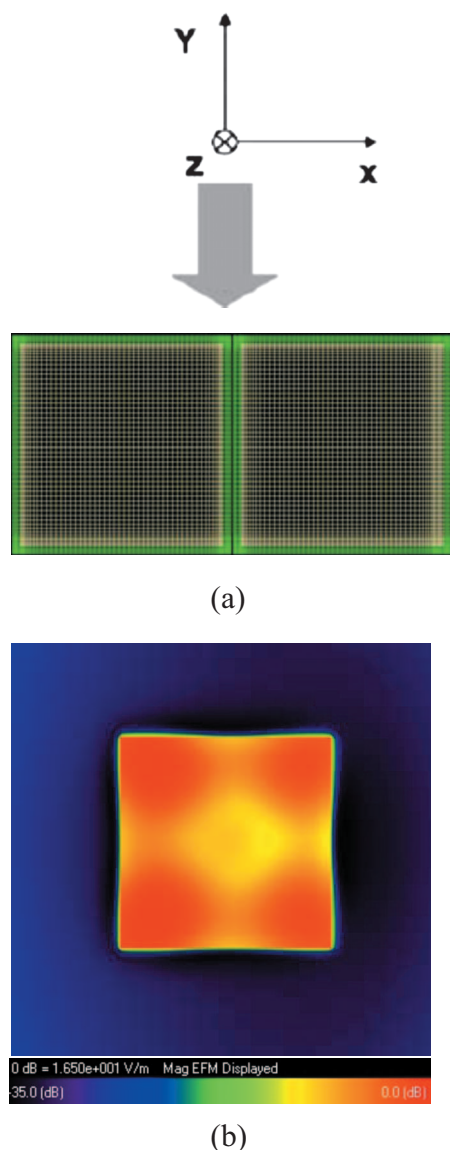


FIG. 8. (Color) FDTD simulations of the near field distribution in the contact plane. The excitation polarization is along the x -axis.

tem should take the near field coupling effect into consideration. So, a model consisting of two Au@Pd nanocubes, rather than a single nanocube, was used in our FDTD simulation [see Fig. 8(a)]. In the calculation, the Au cube core is set to be 83 nm, interparticle shell-shell distance 1 nm. The 632.8 nm monochromatic plane wave is incident from the top (y -axis) with the polarization parallel to the axis along the particle pair (x -axis). The Yee cell size in the shell region is set to be $0.5 \times 0.5 \times 0.5 \text{ nm}^3$ while a $2 \times 2 \times 2 \text{ nm}^3$ cell size is used in other simulation regions. This nonuniform FDTD mesh method can save computation resources greatly without losing accuracy.

Our calculation shows the maximum field enhancement, defined as the ratio between the maximum local field E_{loc} and the incoming field E_{in} amplitude, is about 10–25 depending on the thickness of Pd shell (0–5 nm), and the hot site (most enhanced region) of SERS always exists in the gap region. Since the enhanced Raman scattering intensity from a probe molecule at any given position is approximately proportional to the fourth power of the electric field enhancement at the position of the molecule, so the maximum Raman electromagnetic enhancement factor for a Au@Pd particle dimer can reach from 1.0×10^4 to 3.9×10^5 if the thickness value of Pd shell in the range of 0–5 nm. Figure 8(b) gives a typical field distribution at the junction (yz plane at $x=0$) of two nanocubes with a 1 nm Pd shell. It can be seen the maximal field enhancement is about 16.5, corresponding to 7.4×10^4 of the Raman signal enhancement. This value is higher than that of two pure 83 nm Pd nanocubes. It can be seen clearly that the magnitude of the electric field reaches the maximum in the gap region of the dimer. Since the SERS signal obtained in the experiment should average over all the surfaces, therefore, the enhancement obtained in the experiment may be substantially lower than the calculated value. So, experimental Raman signal enhancement contributed from electromagnetic enhancement is estimated in the order of 10^3 .

The high SERS activity achieved in Au@Pd ultrathin shell systems is attributed to the long-range effect of the enhanced electromagnetic field generated by the Au core. Based on 3D-FDTD method, the dependence of the SERS activity on the Pd shell thickness was quantitatively investigated. The simulated FDTD results (see Fig. 9) reveal that

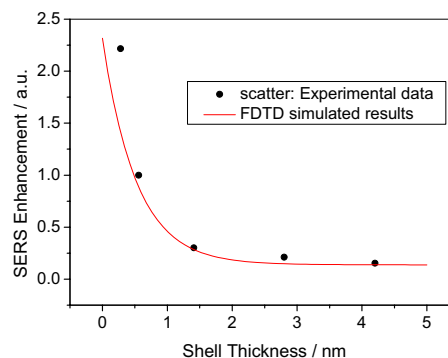


FIG. 9. (Color online) Dependence of the SERS intensity of CO adsorbed on 83 nm Au@Pd nanocubes on the thickness of Pd shell (circles) and the corresponding FDTD calculation result [solid (red) line]. The experimental result is taken from Ref. 30.

the SERS enhancement decreases exponentially with increasing thickness of Pd. This result shows essentially the same trend as the experimental result reported in Ref. 30.

IV. CONCLUSION

With quantum chemical method, generalized Mie theory, and 3D-FDTD method, we investigated SERS of Pyridine adsorbed on Au@Pd Core/Shell Nanoparticles. The theoretical study show Au@Pd core/shell nanoparticles are a good substrate for SERS, and the high SERS activity achieved in ultrathin shell systems is contributed mainly from the long-range effect of the enhanced electromagnetic field generated by the Au core. Static chemical enhancement by CT from pyridine to Au core at the ground state is also discussed in detail. It is noted that the photoinduced charge redistribution takes place at first Pd layer (surface Plasmon from transition metal). When the Pd shell becomes thicker, the absorption peak of the Au core slightly redshifts and damps gradually. The theoretical results reveal that the static chemical enhancement and electromagnetic enhancement are in the order of 10 and 10^3 , respectively.

ACKNOWLEDGMENTS

This work was supported by the National Natural Science Foundation of China (Grant Nos. 10874234, 20703064, 20703032, and 10625418), National Basic Research Project of China (Grant Nos. 2009CB930701, 2009CB930703, and 2007CB936804), Sino-Swedish Collaborations about Nanophotonics and Nanoelectronics (Grant No. 2006DFB02020), Natural Science Foundation of Fujian Province of China (Grant No. E0710028), and “Bairen” projects of CAS.

- ¹M. Fleischmann, P. J. Hendra, and A. J. McQuillan, *Chem. Phys. Lett.* **26**, 163 (1974).
- ²D. L. Jeanmaire and R. P. Van Duyne, *J. Electroanal. Chem. Interfacial Electrochem.* **84**, 1 (1977).
- ³M. G. Albrecht and J. A. Creighton, *J. Am. Chem. Soc.* **99**, 5215 (1977).
- ⁴M. Moskovits, *Rev. Mod. Phys.* **57**, 783 (1985); H. Metiu and P. Dos, *Annu. Rev. Phys. Chem.* **35**, 507 (1984).
- ⁵H. X. Xu, E. J. Bjerneld, M. Kail, and L. Borjesson, *Phys. Rev. Lett.* **83**, 4357 (1999).
- ⁶A. Otto, I. Mrozek, H. Grabhorn, and W. Akemann, *J. Phys.: Condens. Matter* **4**, 1143 (1992).
- ⁷J. R. Lombardi, R. L. Birke, T. Lu, and J. Xu, *J. Chem. Phys.* **84**, 4174 (1986).
- ⁸L. L. Zhao, L. Jensen, and G. C. Schatz, *J. Am. Chem. Soc.* **128**, 2911 (2006).
- ⁹K. Kneipp, H. Kneipp, I. Itzkan, R. R. Dasari, and M. S. Feld, *Chem. Rev. (Washington, D.C.)* **99**, 2957 (1999).
- ¹⁰Z. Q. Tian, B. Ren, J. F. Li, and Z. L. Yang, *Chem. Commun. (Cambridge)* **2007**, 3514 (2007).

- ¹¹C. Li, *Stud. Surf. Sci. Catal.* **170**, 561 (2007).
- ¹²Z. Q. Tian and B. Ren, *Annu. Rev. Phys. Chem.* **55**, 197 (2004).
- ¹³Z. Q. Tian, Z. L. Yang, B. Ren, J. F. Li, Y. Zhang, X. F. Lin, J. W. Hu, and D. Y. Wu, *Faraday Discuss.* **132**, 159 (2006).
- ¹⁴J. F. Li, Z. L. Yang, B. Ren, G. K. Liu, P. P. Fang, Y. X. Jiang, D. Y. Wu, and Z. Q. Tian, *Langmuir* **22**, 10372 (2006).
- ¹⁵K. Zhang, Y. Xiang, X. C. Wu, L. Feng, W. He, J. Liu, W. Zhou, and S. Xie, *Langmuir* **25**, 1162 (2009).
- ¹⁶J. Y. Chen, B. Wiley, J. McLellan, Y. J. Xiong, Z. Y. Li, and Y. N. Xia, *Nano Lett.* **5**, 2058 (2005).
- ¹⁷C. M. Cobley, D. J. Campbell, and Y. N. Xia, *Adv. Mater. (Weinheim, Ger.)* **20**, 748 (2008).
- ¹⁸S. Zou, C. T. Williams, E. K. Y. Chen, and M. J. Weaver, *J. Am. Chem. Soc.* **120**, 3811 (1998).
- ¹⁹S. Zou and M. Weaver, *J. Anal. Chem.* **70**, 2387 (1998).
- ²⁰F. Y. Chen and R. L. Johnson, *Appl. Phys. Lett.* **90**, 153123 (2007).
- ²¹L. Jensen, L. L. Zhao, and G. C. Schatz, *J. Phys. Chem. C* **111**, 4756 (2007).
- ²²M. Pagliai, L. Bellucci, M. Muniz-Miranda, C. Cardini, and V. Schettino, *Phys. Chem. Chem. Phys.* **8**, 171 (2006).
- ²³M. T. Sun, S. Liu, M. Chen, and H. X. Xu, *J. Raman Spectrosc.* **40**, 137 (2009).
- ²⁴M. T. Sun, S. Liu, Z. P. Li, J. M. Duan, M. Chen, and H. X. Xu, “Direct visual evidence for the chemical mechanism of surface-enhanced resonance Raman scattering via charge transfer: (11) Binding-site and quantum-size effects,” *J. Raman Spectrosc.* (in press) DOI:10.1002/jrs.2255.
- ²⁵H. X. Xu, *J. Opt. Soc. Am. A Opt. Image Sci. Vis* **21**, 804 (2004).
- ²⁶K. S. Kunz and R. J. Luebber, *The Finite Difference Time Domain Method for Electromagnetics* (CRC, Cleveland, 1993).
- ²⁷M. T. Sun and H. X. Xu, *ChemPhysChem* **10**, 392 (2009).
- ²⁸J. Li, X. Li, H. J. Zhai, and L. S. Wang, *Science* **299**, 864 (2003).
- ²⁹L. L. Zhao, L. Jensen, and G. C. Schatz, *Nano Lett.* **6**, 1229 (2006).
- ³⁰J. J. Sheng, J. F. Li, B. S. Yin, B. Ren, and Z. Q. Tian, *Can. J. Anal. Sci. Spectrosc.* **52**, 178 (2007).
- ³¹M. J. Frisch, G. W. Trucks, H. B. Schlegel *et al.*, GAUSSIAN 03, Revision E.01, Gaussian, Wallingford, 2004.
- ³²P. Hohenberg and W. Kohn, *Phys. Rev.* **136**, B864 (1964).
- ³³A. D. Becke, *J. Chem. Phys.* **98**, 5648 (1993); C. Lee, W. Yang, and R. G. Parr, *Phys. Rev. B* **37**, 785 (1988).
- ³⁴P. J. Hay and W. R. Wadt, *J. Chem. Phys.* **82**, 270 (1985).
- ³⁵N. O’Boyle, GaussSum, Revision 2.1, <http://GaussSum.sf.net>.
- ³⁶E. K. U. Gross and W. Kohn, *Phys. Rev. Lett.* **55**, 2850 (1985).
- ³⁷J. Sinzig and M. Quinten, *Appl. Phys. A* **58**, 157 (1994).
- ³⁸H. X. Xu, *Phys. Rev. B* **72**, 073405 (2005).
- ³⁹A. Vial and T. Laroche, *J. Phys. D* **40**, 7152 (2007).
- ⁴⁰P. G. Etchegoin, E. C. Le Ru, and M. Meyer, *J. Chem. Phys.* **125**, 164705 (2006).
- ⁴¹F. Hao and P. Nordlander, *Chem. Phys. Lett.* **446**, 115 (2007).
- ⁴²J. T. Krug II, E. J. Sanchez, and X. S. Xie, *J. Chem. Phys.* **116**, 10895 (2002).
- ⁴³Z. Q. Tian, Z. L. Yang, B. Ren, and D. Y. Wu, *Top. Appl. Phys.* **103**, 125 (2006).
- ⁴⁴P. B. Johnson and R. W. Christy, *Phys. Rev. B* **6**, 4370 (1972).
- ⁴⁵E. D. Palik, *Handbook of Optical Constants of Solids* (Academic, New York, 1985).
- ⁴⁶D. Y. Wu, M. Hayashi, S. H. Lin, and Z. Q. Tian, *Spectrochim. Acta, Part A* **60**, 137 (2004).
- ⁴⁷P. P. Fang, J. F. Li, Z. L. Yang, L. M. Li, B. Ren, and Z. Q. Tian, *J. Raman Spectrosc.* **39**, 1679 (2008).